J Mater Sci (2011) 46:5503–5511
DOI 10.1007/s10853-011-5494-8

Swelling of 316L austenitic stainless steel induced by plasma nitriding

J. C. Stinville · C. Templier · P. Villechaise · L. Pichon

Received: 25 January 2011 / Accepted: 21 March 2011 / Published online: 2 April 2011

Abstract Swelling of 316L austenitic stainless steel plasma nitrided at 400°C under floating potential has been investigated using electron back scattered diffraction and white-light interferometry. Swelling of individual grains strongly depends on their crystallographic orientation, similarly to the thickness of the nitrided layer. After 1 h of treatment, swelling is maximum for the ⟨001⟩ oriented grains and minimum for the ⟨111⟩ oriented grains. After 8 and 33 h of nitriding, the maximum of swelling is observed in the grains having their normal direction at about 15° from the ⟨001⟩ orientation. These results are discussed on the basis of plastic strain after comparison with calculated swellings of the ⟨001⟩ and ⟨111⟩ oriented grains, using the thickness of the nitrided layer deduced from the trapping–detrapping diffusion model and a rough estimation of the plastic strain. The satisfactory agreement between experimental and calculated swellings supports the idea that swelling results from the lattice expansion due to the incorporation of nitrogen plus an elastic strain and a plastic strain. For individual grains of the 316L matrix, nitriding leads to a tensile-like elongation of high magnitude (around 20%) and it might be the origin of the lattice rotations which were previously observed after nitriding.

J. C. Stinville · C. Templier (✉) · P. Villechaise · L. Pichon
Institut PPRIME, CNRS UPR 3346, Université de Poitiers & ENSMA, BP 30179, 86962 Futuroscope-Chasseneuil, France
e-mail: claude.templier@univ-poitiers.fr

J. C. Stinville
e-mail: jean-charles.stinville.1@ens.etsmtl.ca

Present Address:
J. C. Stinville
Ecole de Technologie Supérieure, 1100 rue Notre-Dame Ouest, Montreal, QC, Canada

Abbreviations

ASS	Austenitic stainless steel
NRA	Nuclear reaction analysis
EBSD	Electron backscattered diffraction
NRA	Nuclear reaction analysis
GDOES	Glow discharge optical emission spectroscopy
FEG	Field emission gun
SEM	Scanning electron microscope
WLI	White light interferometry
ND	Normal direction
IPF	Inverse pole figure
IQ	Image quality

Introduction

Nitriding of austenitic stainless steels (ASS) is used to improve their mechanical resistance [1, 2]. At moderate temperature, it leads to the formation of a modified layer retaining the structure of the host matrix [3, 4] with the incorporation of nitrogen atoms in the octahedral sites of the host matrix [5]. Among the microstructural modifications, it induces crystallographic rotation which amplitude and direction depend on both the N concentration and the initial orientation of the grain [6, 7]. The trend of the observed lattice rotations in the nitrided region is very similar to that occurring in aluminium submitted to tensile elongation [8, 9]. The most obvious process leading to the elongation-like of the nitrided region is the expansion of the stress-free lattice parameter, which depends on the fraction of the interstitial sublattice occupied by nitrogen atoms [10]. This expansion is about 9% at the surface for a nitrogen concentration of ~33 at.%. It is continuously

decreasing across the nitrided region, in relation with the nitrogen concentration profile. Thus, the lattice expansion due to nitrogen incorporation is likely not sufficient to describe the effective matrix elongation. This matrix elongation can be experimentally deduced from both the thickness of the nitrided region and the swelling, i.e., the displacement of the surface from its initial position. Nitrogen diffusion depth being dependent on the grain orientation [11, 12], the experimental swelling was investigated for individual grains of nitrided ASS 316L. The swelling was also estimated using a theoretical approach combining diffusion in the presence of traps [13, 14] and conservation of the expanded volume in the presence of residual stresses.

Experimental details

The material investigated was a 316L type polycrystalline austenitic stainless steel (AISI 316L, AFNOR 23 CND 17-12) with an average grain size of 50 μm. Details on the sample surface preparation to suppress potential work-hardening and to ease electron backscattered diffraction (EBSD) have been given in a previous paper [6]. The 316L specimens were nitrided in the URANOS plasma system [15] in which plasma is created by a 13.56 MHz electromagnetic excitation with a forward input power of 700 W, specimens being maintained at floating potential (a few volts). Sputtering of the surface of the samples is thus negligible. Nitriding was performed at 400°C and at a working pressure of 7.5 Pa using a flow of 60 sccm N_2 plus 40 sccm H_2 for various durations ranging from 1 to 33 h.

Nitrogen profiles were determined either by nuclear reaction analysis (NRA, made at FZD, Rossendorf, Germany) or glow discharge optical emission spectroscopy (GDOES). EBSD was performed on a scanning electron microscope (SEM) JEOL 6100 (acceleration voltage 25 kV) equipped with an orientation imaging microscopy system (OIM) commercialized by TSL, as described in Ref. [6]. Surface topography was investigated using a JEOL JSM 7000F field emission gun scanning electron microscope (FEG-SEM) operating in the 15–25 kV range and a Talysurf CCI 6000 3D optical profiler operating with Mireau interference objectives and white light source. The investigated areas were 900×900 or 360×360 μm^2 ($\times 20$ or $\times 50$ objective, respectively) with lateral resolution lower than 1 μm and expected vertical resolution of about 0.1 nm. Registered and stitched images were numerically processed using Talymap software V4.1 thus providing 3D profiles of large areas within the 2 mm^2 zones investigated by EBSD.

Experimental results

Swelling of the nitrided grains

Figure 1 presents a SEM surface view of a specimen nitrided for 3 h. Together with the appearance of slip bands, it illustrates the grain-to-grain swelling with a step-like about 0.6 μm high at a grain boundary. Specific swelling is observed close to the grain boundaries and only the swelling of the near centre of the grains has been considered in the following part, avoiding the effect of neighbouring grains.

Figure 2 is a white light interferometry (WLI) observation of the surface of the sample nitrided for 3 h. The use of $\times 50$ objective allows to appreciate the average roughness R_a within grains, which is found close to 50 nm, well below the height difference (~ 0.4 μm) between the grains. The average roughness R_a within grains has been evaluated for many grains for the various nitriding durations; it does not exceed 100 nm for the 33 h nitrided sample and is only 30 nm for 1 h nitrided sample. This roughness is mostly due to the slip bands (see Fig. 1) resulting from plastic deformation in the nitrided region of the grains [16–18]. Consequently, the height of individual grains has been obtained by smoothing the height values over their quite entire surface, a zone close to their boundaries being excluded. Only grains with size larger than 20 μm were taken into account to omit neighbouring effect.

For each investigated sample, the surface of reference for the estimate of the swelling was the few mm^2 surface hidden during nitriding using a ~ 5 mm^2 mask made from a 0.5 mm thick silicon wafer. The produced step between the masked and nitrided surface for the 33 h nitrided specimen is shown on Fig. 3, which is a WLI observation

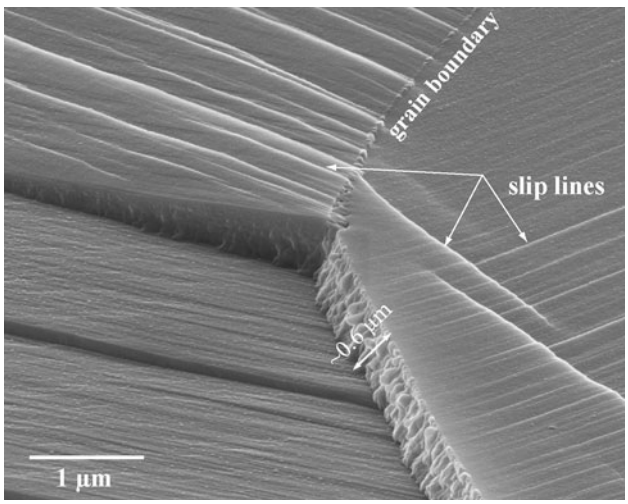

Fig. 1 SEM images (tilt 70°) of the surface showing the resulting grain-to-grain swelling after 3 h of nitriding

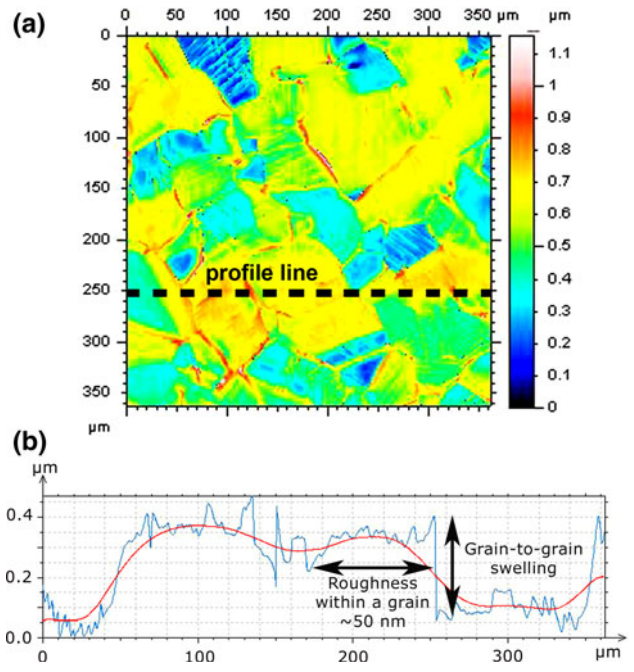

Fig. 2 WLI observation (×50 objective) of the surface of the sample nitrided for 3 h (**a**) and *line profiling* showing the roughness within grains and the height difference between the grains (**b**). The *red curve* results from a smoothing of the profile line

with the ×20 objective. Resulting from the mechanical–chemical polishing with colloidal silica, roughness in the masked zone is in the nm range, much lower than the roughness in the overall nitrided zone which is in the µm range, resulting from the nonuniformity in the swelling behaviour of the investigated grains.

Close to the edge of the masked zone, a border region about 400 µm wide exhibiting shadowing effect was excluded. After stitching of 900 × 900 µm^2 zones obtained with the ×20 objective, a representative image gathering more that 1,000 grains was used to estimate the maximum and minimum swellings, defined as the averaged value of the ten highest or lowest height values, respectively. As shown on Fig. 4, these swellings quite linearly increase with the square root of the nitriding duration and the maximum swelling reaches 3.5 µm for the longest nitriding duration of 33 h. The experimental values of these swellings are gathered in Table 1.

White light interferometry and EBSD measurements on the same zone of the sample nitrided were combined to investigate the relationship between the swelling of a grain and its orientation. The orientation of a grain is given by its ND direction, i.e., the direction normal to the surface. As observed on Fig. 5 for 1 h of treatment, swelling significantly depends on the initial orientation of the grains: the swelling of the near oriented ⟨100⟩ grains (near red colour) is higher than the swelling of the near oriented ⟨111⟩ or ⟨101⟩ grains (near blue or green colour, respectively).

The dependence of swelling on the ND orientation can be also described using the differential swelling, defined as the difference between the swelling SW_{hkl} of a ⟨*hkl*⟩ oriented grain and the minimum swelling. This has been measured for about one hundreds grains in the 2 mm^2 area

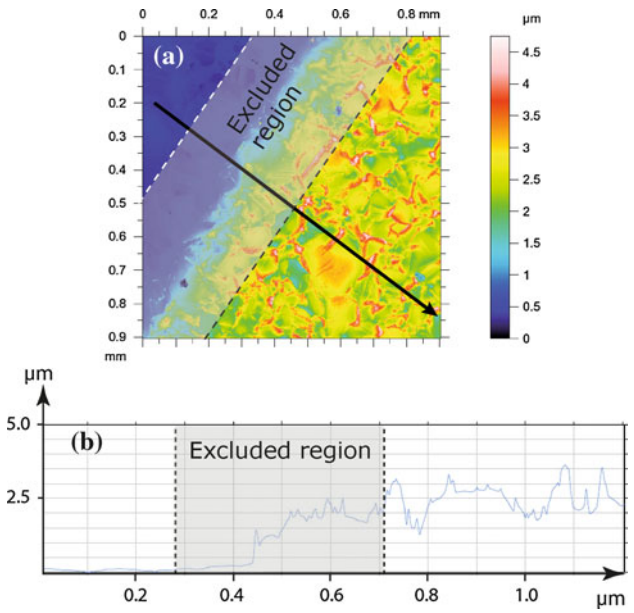

Fig. 3 WLI investigations (900 × 900 µm2, ×20 objective) of the step height between masked zone (in *blue*) and nitrided zone of sample nitrided for 33 h. The height profile (**b**) corresponds to the *arrow* indicated on (**a**)

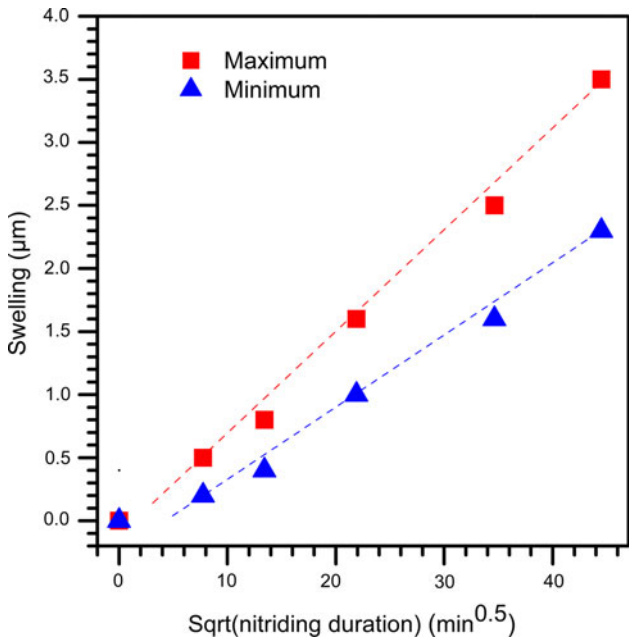

Fig. 4 Maximum and minimum swellings versus the square-root of the nitriding duration (*lines* are guide for the eyes)

Table 1 Nitrogen surface concentration, maximum and minimum thicknesses of the nitrided layer; maximum and minimum swellings and elongations for the various treatment durations

Nitriding duration	1 h	3 h	8 h	20 h	33 h
Nitrogen surface concentration (at.%)	28 ± 2	33 ± 2	33 ± 2	33 ± 2	33 ± 2
X_{001}: Thickness in ⟨001⟩ grains (μm), from SEM/EBSD	3.6 ± 0.5		12.0 ± 0.5		21 ± 1
X_{111}: Thickness in ⟨111⟩ grains (μm), from SEM/EBSD	3.0 ± 0.5		7.7 ± 0.5		14 ± 1
Maximum ($\sim X_{001}$) thickness (μm) of the nitrided layer (at 1 at.%) from GDOES profiles	3.9 ± 0.5	6.0 ± 0.5	11 ± 1	15 ± 1	20 ± 1
Minimum ($\sim X_{111}$) thickness (μm) of the nitrided layer (at 13 at.%) from GDOES profiles	3.0 ± 0.5	4.3 ± 0.5	6.8 ± 0.5	8.4 ± 0.5	13 ± 1
Minimum swelling or SW_{111} (μm)	0.20 ± 0.05	0.4 ± 0.1	1.0 ± 0.2	1.6 ± 0.2	2.3 ± 0.2
Maximum swelling (μm)	0.5 ± 0.1	0.8 ± 0.1	1.6 ± 0.2	2.5 ± 0.2	3.5 ± 0.2
Swelling SW_{001} (μm)	0.5 ± 0.2	0.8 ± 0.2	1.5 ± 0.3	2.3 ± 0.3	3.2 ± 0.3
Elongation $\Gamma_{\langle 001\rangle}$ (%)	15 ± 7	15 ± 5	16 ± 4	18 ± 3	19 ± 3
Elongation $\Gamma\langle 111\rangle$ (%)	7 ± 3	10 ± 4	17 ± 4	24 ± 4	21 ± 4

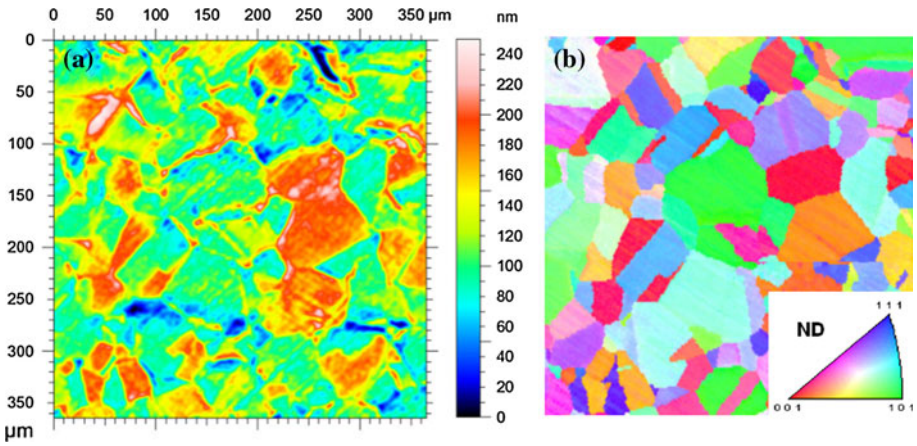

Fig. 5 Investigation on the 1 h nitrided sample: **a** WLI observations (360 × 360 μm^2, ×20 objective) and **b** associated EBSD measurements, similarly colour coded as shown on the *colour bar* and the inserted ND inverse pole figure

investigated by EBSD, and it is presented on Fig. 6a–c for three different durations of nitriding, using ND inverse pole figures (IPF). On the IPF, the locations of the symbols used to describe the amplitude of the differential swelling correspond to the initial orientation of the grains. It is observed that the differential swelling for a given orientation increases with the duration of nitriding. The lowest values of the differential swellings corresponds to the near ⟨111⟩ oriented grains. After 1 h of nitriding, the grains closely oriented to ⟨001⟩ exhibit the largest differential swellings. However, for higher durations of treatment, the maximum swellings are observed for grains which initial orientations differs from ⟨001⟩, corresponding to the grey tint regions on Fig. 6b, c. Another way to represent the dependence on the grain orientation is to plot the differential swelling versus $\theta_{\langle 001\rangle}$, the minimum angle between the ⟨001⟩ direction and its ND direction. As shown on Fig. 6d, there is a monotonous dependence after 1 h of nitriding, while for longer durations of treatment a break is observed around $\theta_{\langle 001\rangle} = 15°$, corresponding to the grey tint region on the IPF.

Elongation of the nitrided region

NRA and GDOES average both the grain-to-grain thickness of the nitrided region and N surface concentration. According to the NRA measurements in 316L single crystals [12], there is no drastic dependence of the N surface concentration on the grain orientation and NRA gives an acceptable mean value of this concentration (Table 1). The dependence on grain orientation of the thickness of the nitrided region is more pronounced. In plasma nitrided Inconel 690, He et al. [11] reported a quite linear decrease of this thickness from ∼5 μm for $\theta_{\langle 001\rangle} = 0$ (⟨001⟩ oriented grains) till ∼2 μm at $\theta_{\langle 001\rangle} = 54.7°$ (⟨111⟩ oriented grains). This behaviour was also observed in plasma nitrided 316L using cross-sectional samples, the nitrided region being imaged by mapping the quality index (IQ) of the EBSD patterns as illustrated on Fig. 7 for the 33 h nitrided sample. An orientation-dependent thickness is clearly observed. Moreover, within a grain, the thickness is larger or smaller close to the grains boundaries, depending on the orientation of the neighbouring grains [11].

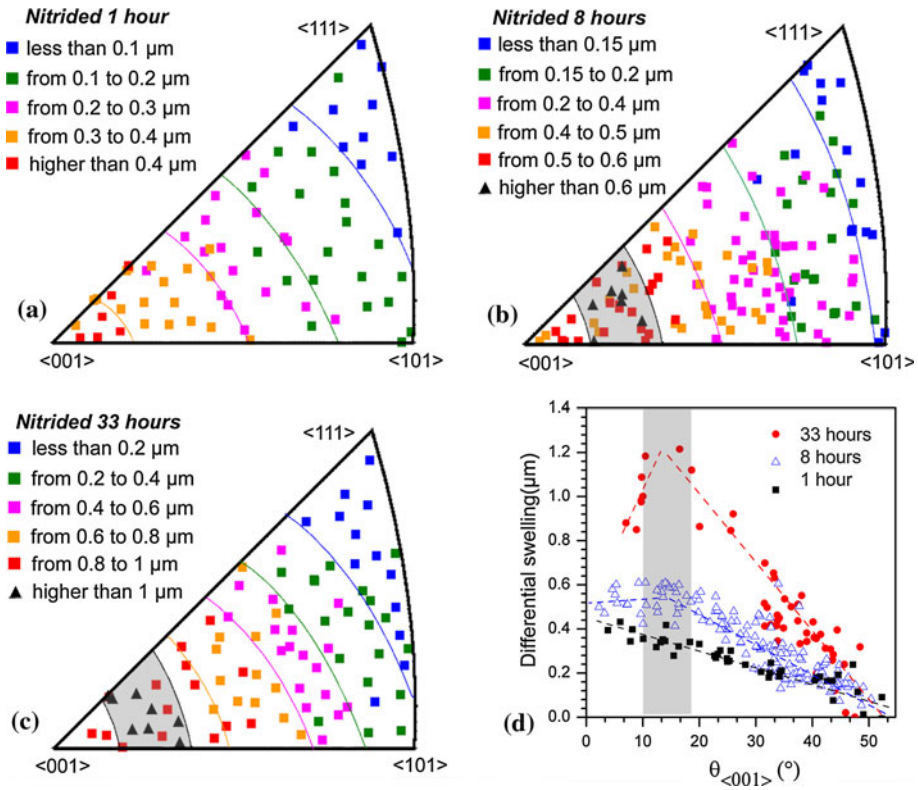

Fig. 6 The grain-to-grain differential swelling according to the grain orientation (**a**–**c**) using ND inverse pole figures and **d** versus $\theta_{\langle 001\rangle}$ (the minimum angle between the $\langle 001\rangle$ direction and the $\langle hkl\rangle$ direction in the crystal lattice in a grain) for 1, 8, and 33 h of nitriding

However, depth could be considered constant far from the grain boundaries and the thicknesses reported in Table 1 were estimated at equal distance from these boundaries. The orientation of each grain was identified by its initial ND direction (i.e., its $\theta_{\langle 001\rangle}$ value), deduced from EBSD investigation within the 316L matrix, a few µm below the interface. About 30 grains were investigated for each conditions of treatment and results are presented on Fig. 8a.

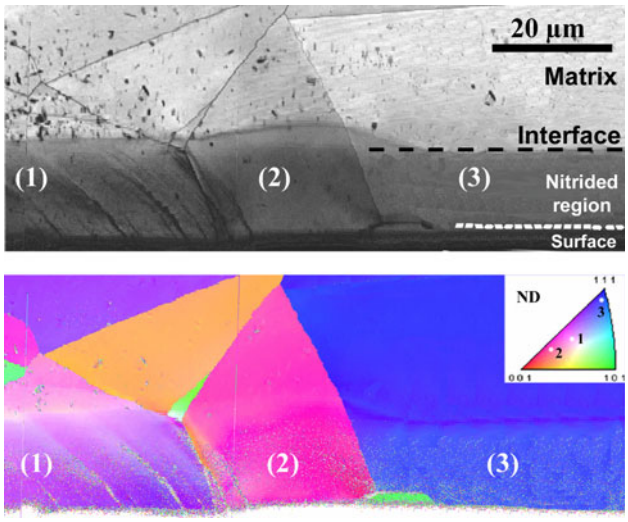

Fig. 7 EBSD pattern on a cross section of the sample nitrided for 33 h: IQ (index quality) map showing the nitrided region in three grains (1, 2, 3) with orientations shown in the ND inverse pole figure inserted in the EBSD map

Similarly to the observations in Inconel 690 [11], there is a quasi linear dependence of the thickness of the nitrided region on the angle $\theta_{\langle 001\rangle}$, the slope being apparently higher pronounced for the larger thicknesses, i.e., the larger durations of treatment. Despite the technique averaged profiles of numerous grains with various orientations, the grain-to-grain thickness can be estimated from GDOES profiling. Indeed, for the three investigated durations (1, 8, and 33 h), the thickness in the $\langle 001\rangle$ oriented grains, determined from EBSD on cross-sections, corresponds to the depth at which N concentration is about 1 at.% on the GDOES profiles while the thickness of the $\langle 111\rangle$ oriented grains corresponds to about 13 at.%. It gives criteria to estimate the thickness for the samples nitrided for 3 and 20 h which were not investigated using cross-sectional samples. These estimated values are given in Table 1 as well as the corresponding EBSD measurements on cross-sectional samples. The thickness of the nitrided layer and the related swelling are represented as a function of the square-root of the nitriding duration on Fig. 8b, c.

The elongation Γ_{hkl} of the nitrided region for a $\langle hkl\rangle$ oriented grain is defined as $SW_{hkl}/(X_{hkl} - SW_{hkl})$, where X_{hkl} is the thickness of this region. It was calculated for the $\langle 001\rangle$ and $\langle 111\rangle$ oriented grains (see Table 1) using X_{hkl} deduced from the GDOES results. This elongation firstly

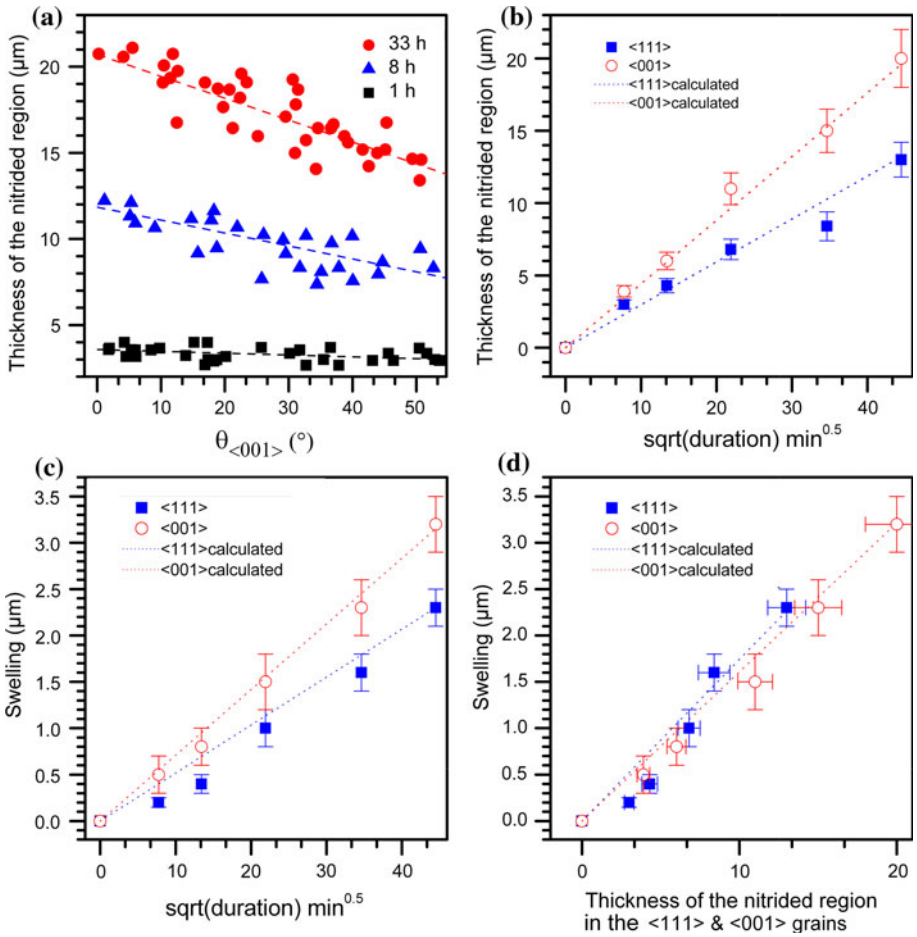

Fig. 8 Thickness of the nitrided region (**a**) as a function of $\theta_{\langle 001\rangle}$ (*lines* are guides for the eyes), thickness (**b**), and swelling (**c**) versus the square-root of the nitriding duration, and swelling (**d**) versus the thickness for the $\langle 111\rangle$ and $\langle 001\rangle$ oriented grains (*lines* correspond to the calculated values)

increases with the nitriding duration and stays around 20% after 8 h of nitriding.

Discussion

The magnitude of the estimated elongation ($\sim$20%) is well above the expansion resulting from the introduction of nitrogen in the 316L lattice, even taking into account the presence of in-plane biaxial residual stresses which induces a negative elastic strain parallel to the surface and a positive elastic strain in the normal direction [19]. Thus, some other processes are necessary to explain such elongation and this is likely plastic strain as revealed by the presence of the slip bands on the surface (see Fig. 1). It suggests a simple approach to evaluate a theoretical swelling of a $\langle hkl\rangle$ oriented grain (see Appendix). Expansion A of the matrix lattice at a given depth could be obtained from the calculated N concentration profiles. The elastic strain originating from the residual stresses can be deduced using the elastic properties. The plastic strain can be roughly estimated assuming the conservation of the expanded volume: parallel swelling is indeed inconceivable since each grain is blocked by its neighbours and swelling mostly occurs in the direction normal to the free surface. Experimental observations confirm that there is no drastic modification of the morphology of the grains on the surface, except close to the grain boundaries. If these grain boundary effects play a role in the development of surface damage as intergranular cracks or extrusion, they can be neglected for the present analysis as the experimental swelling and thickness were estimated excluding the zones around grain boundaries.

The calculation of the N concentration profiles has been made using the trapping–detrapping model [20]. As only quite long nitriding durations are investigated in the present study and that it was done to get the relationship between the thickness of the nitrided layer and the swelling, the calculations were performed assuming a constant surface N concentration of 33 at.%. Thus, the only parameter was the diffusion coefficient D_{hkl} [12]. Profiles were calculated for the $\langle 001\rangle$ and $\langle 111\rangle$ oriented grains by adapting the diffusion coefficient such that the calculated thickness after 33 h reasonably fits the experimental ones (Table 1). The other parameters were identical to those given in Ref. [12]. Swelling, evaluated

following the Appendix, was taken into account as a part of the thickness of the nitrided layer.

The dotted lines on Fig. 8b and c represent the results of the calculations for the thicknesses and swellings for the ⟨001⟩ and ⟨111⟩ oriented grains, using $D_{001} = 1.4 \times 10^{-11}$ cm^2 s^{-1} and $D_{111} = 0.7 \times 10^{-11}$ cm^2 s^{-1}. The fact that the ratio of the diffusion coefficients is similar to the ratio obtained by Martinavicius et al. [12] for the fitting of N concentration profiles in ⟨111⟩ and ⟨001⟩ single crystals gives some validity to the employed approach, i.e., calculations with a constant surface concentration. The calculated swelling based on the assumption that the expanded volume is mostly retained (it is slightly modified by the residual stresses) is in satisfactory agreement with the experimental observations. Moreover, Fig. 8d indicates that the swelling is almost proportional to the thickness of the nitrided layer. For the long nitriding durations or, equivalently, the high thicknesses, experimental values lie close to the dashed line corresponding to the calculated values. It indicates that in this range of thickness, plasticity is the main process which, in parallel with the expansion, contributes to the elongation of the matrix in the direction normal to the sample surface.

Obviously, there is, however, a discrepancy for the lowest investigated thicknesses, especially for the ⟨111⟩ oriented grains. The employed rudimentary approach, based on the volume conservation, does not take into account the mechanisms of plasticity, which do not operate until the resolved shear stress reaches a critical value. This critical value of the resolved shear stress likely corresponds to a critical value of the occupancy of the octahedral sites by the N atoms. It means that plasticity is initiated close to the nitriding front where the nitrogen concentration drastically increases from 0 to ~15 at.% and later develops through the entire nitrided layer as this nitriding front moves forward. For the thin nitrided layers, what happens in the region close to the nitriding front likely strongly affects the kinetics of plasticity. However, for the thick nitrided layer, initiation of plasticity within the nitriding front is more and more hidden by the development of the plasticity in the overall nitrided layer. Consequently, the approach based on the conservation of the volume becomes more and more appropriate as the thickness increases.

It is commonly assumed that the critical value of the resolved shear stress does not depend on the grain orientation. However, the yield strength depends on the orientation and this effect can be expressed through the Schmid factor. In an ASS as in its expanded γ_N phase, dislocation glide occurs along the ⟨110⟩ directions in ⟨111⟩ plans and the Schmid factor for the ⟨111⟩ oriented grains is lower than that of the ⟨001⟩ oriented grains. It might explain why the experimental swelling is so low (~7%) and close to the expansion for the ⟨111⟩ grains after 1 h of nitriding, plasticity starting first in the ⟨001⟩ oriented grains.

The fact that the maximum of swelling occurs not for the ⟨001⟩ grains, which exhibit the maximum thickness of the nitrided region, but for grains oriented such that $\theta_{\langle 001 \rangle} \approx 15°$ could be also related to the corresponding larger value of the Schmid factor. Indeed, it is likely more complicated as it was observed during uniaxial tensile loading of a stainless steel that the onset of plasticity occurs in grains oriented such that they exhibit the largest number of slips systems [21]. Besides, it has been recently observed that nitriding affects the anisotropy of the elastic modulus [22]. In 316L, E_{hkl} quite linearly increases from E_{001} till E_{111}. In the nitrided region, E_{111} remains almost the same as in 316L but has the lowest value, E_{hkl} linearly decreasing from E_{001} till E_{111}. This reversal of the anisotropy of E_{hkl} might counterbalance the effect of the Schmid factor corresponding to the initial orientation. Besides, nitrogen is likely not distributed at random but in some extent linked with Cr atoms [23, 24]. Thus, the observed maximum of swelling close to $\theta_{\langle 001 \rangle} \approx 15°$ after 33 h of treatment presumably results from concomitant and interdependent processes (diffusion, onset of phase transformation, plasticity, lattice rotations, residual stresses…) and cannot be deciphered without additional investigations and modelling.

Finally, from a mechanical point of view, the introduction of nitrogen in the interstitial sites of an austenitic stainless steel can be considered equivalent to a tensile load in the direction normal to the surface. It leads to elastic and plastic strains, the later inducing crystallographic lattice rotations.

Conclusion

Swelling of individual grains of nitrided 316L ASS was obtained using combined EBSD and WLI investigations. Similarly to the thickness of the nitrided region, swelling SW_{hkl} of a grain strongly depends on its orientation, SW_{001} being about 1.5 times SW_{111} after 33 h of nitriding. The very satisfactory agreement between calculated and experimental swellings strongly supports that it results from the expansion of the matrix plus the elastic strain due to the residual stresses (minor effects) plus the plastic strain of the γ_N phase. The magnitude of the elongation (about 20%) also suggests that the observed high level of lattice rotations results from this tensile-like deformation. The amount and direction of lattice rotations for the "deformation" level obtained in the present study (~20%) will be compared to the values predicted by the Taylor model [25, 26] in a forthcoming paper.

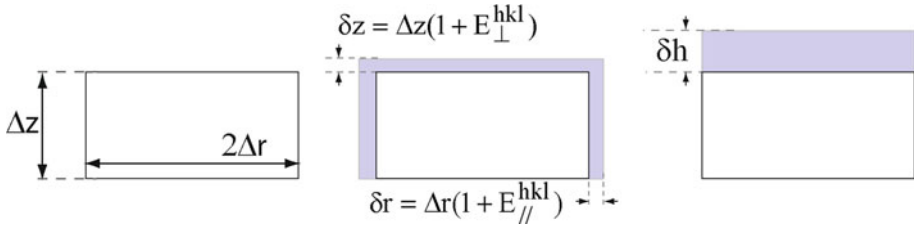

Fig. 9 Schematic view illustrating the simple approach to evaluate the swelling using the conservation of the volume

Furthermore, the simple approach which was used in this study indicates that plasticity should be taken into account when studying the development of the nitrided layer as it induces about ~10% of its thickness. However, further studies are needed for the initial stages, using a more realistic description of the onset and development of plasticity, i.e., by coupling a model for the diffusion of nitrogen with crystal plasticity modelling.

Appendix

The calculation of the elongation taking into account the plastic strain is based on the conservation of the volume of the expanded phase in the presence of stresses. Before nitriding, let us consider a cylindrical elementary volume $\Delta V_i = \pi \Delta r^2 \Delta z$ at a depth z beneath the surface. After the introduction of nitrogen, a new expanded volume $\Delta V_f = \pi(\Delta r + \delta r)^2(\Delta Z + \delta z)$ is obtained. It is assumed that the volume change occurs exclusively through the swelling δh towards the surface as the nitrided region within a grain is constrained by the neighbouring grains. The expansion of the γ phase due to nitrogen insertion, the elastic strain of the γ_N phase due to residual stresses, the total resulting dilatation and the elongation are denoted $A(z)$, $\varepsilon(z)$, $E(z)$ and $\Gamma(z)$, respectively. Using the conservation of the expanded volume schematically described on Fig. 9, simple geometrical considerations give:

$$\Gamma_{hkl}(z) = \frac{\delta h}{\Delta z} = \left(1 + E^{hkl}_{//}(z)\right)^2 \left(1 + E^{hkl}_{\perp}(z)\right) - 1 \qquad (1)$$

where $E^{hkl}_{//}$ and $E^{hkl}_{\perp}$ are the dilatations parallel and normal to the surface, respectively. These dilatations are the sum of the contribution of the expansion A of the lattice parameters, due to the nitrogen insertion, and of the elastic strains ε due to the residual compressive stresses.

According to Christiansen and Somers [10], the expansion $A(z)$ (%) resulting from the introduction of nitrogen in the octahedral sites can be approximated by:

$$A(z) = \frac{\alpha}{a^0(\gamma)} C_N(z) \qquad (2)$$

where $a^0(\gamma)$ is the stress-free lattice parameter of the γ phase, α (nm/at.%) the expansion coefficient and $C_N(z)$ (at.%) the nitrogen concentration, calculated using the trapping–detrapping model [13, 14]. The parameter α depends on the occupancy of the octahedral sites [10] and the value of 9×10^{-4} nm/at.% used in this study was established only for nitrogen concentration C_N higher than ~13 at.%. However, C_N is sometimes lower than ~13 at.%, everywhere inside the nitrided layer in the beginning of the treatment and at the nitriding front when the steady-state concentration on the surface is reached. As our experiments concern nitriding durations higher than 1 h and as thickness of the nitrided region is well above the width of the nitriding front, keeping only one value for the expansion parameter α whatever the N concentration has likely negligible effect on the calculated values.

Expansion is accompanied by the development of high compressive stresses as the nitrided region within a grain is constrained by the neighbouring grains. In the presence of bi-axial in-plane residual compressive stresses σ, the parallel and normal elastic strains $\varepsilon^{hkl}_{//}$ and $\varepsilon^{hkl}_{\perp}$ of the expanded phase γ_N are given by:

$$\varepsilon^{hkl}_{\perp} = 2S^{(1)}_{hkl}\sigma \qquad (3)$$

$$\varepsilon^{hkl}_{//} = 2S^{(1)}_{hkl}\sigma + \frac{1}{2}S^{(2)}_{m}\sigma \qquad (4)$$

where $S^{(1)}_{hkl}$ is the X-rays elastic constant (XEC) for a ND hkl-oriented grain, while $S^{(2)}_{m}$ is an averaged value of the XECs. Following a recent work of Christiansen and Somers, a residual stress gradient was used with a maximum of −2.5 GPa on the surface [27]. Calculations of the elastic strains ε_{hkl} should be done with the XECs of the expanded austenite, which differs from those of the 316L matrix [22] but are not known. However, the present calculations show that stresses have minor effects on the swelling as the negative elastic strain parallel to the surface mostly compensates the positive elastic strain in the normal direction. Thus, XECs of the 316L matrix as given in Ref. [28] were used in the present approach.Combining the expansion and the elastic strain contributions gives:

$$E^{hkl}_{//} = A + \varepsilon^{hkl}_{//}(1 + A) \text{ and } E^{hkl}_{\perp} = A + \varepsilon^{hkl}_{\perp}(1 + A) \qquad (5)$$

Finally, the total elongation is calculated from the sum over the nitrided zone of the $\Gamma(z)$ estimated from Eq. 1, using a finite difference method.

References

1. Reis R, Maliska A, Borges P (2011) J Mater Sci 46:846. doi: 10.1007/s1085301048273
2. Nascimento F, Lepienski C, Foerster C, Assmann A, Da Silva S, Siqueira M, Chinelatto A (2009) J Mater Sci 44:1045. doi: 10.1007/s108530083211z
3. Sun Y, Li X, Bell T et al (1999) J Mater Sci 34:4793. doi: 10.1023/A:1004647423860
4. Lei M (1999) J Mater Sci 34:5975. doi:10.1023/A:1004728711459
5. Gontijo L, Machado R, Miola E, Casteletti L, Alcântara N, Nascente P et al (2006) Mater Sci Eng A 431:315
6. Stinville J, Villechaise P, Templier C, Rivière J, Drouet M et al (2010) Acta Mater 58:2814
7. Templier C, Stinville J, Villechaise P, Renault P, Abrasonis G, Rivière J, Martinavičius A, Drouet M et al (2010) Surf Coat Technol 204:2551
8. Winther G, Margulies L, Schmidt S, Poulsen H et al (2004) Acta Mater 52:2863
9. Han J, Kim D, Jee K, Oh K et al (2004) Mater Sci Eng A 387–389:60
10. Christiansen T, Somers M et al (2006) Metallu Mater Trans A 37:675
11. He H, Czerwiec T, Dong C, Michel H et al (2003) Surf Coat Technol 163–164:331
12. Martinavičius A, Abrasonis G, Möller W, Templier C, Riviére JP, Declémy A, Chumlyakov Y (2009) J Appl Phys 105:093502
13. Parascandola S, Möller W, Williamson D et al (2000) Appl Phys Lett 76:2194
14. Christiansen T, Dahl K, Somers M et al (2008) Mater Sci Technol 24:159
15. Perrière J, Siejka J, Rémili N, Laurent A, Straboni A, Vuillermoz B et al (1986) J Appl Phys 59:2752
16. Xiaolei X, Liang W, Zhiwei Y, Zukun H et al (2005) Surf Coat Technol 192:220
17. Leroy C, Czerwiec T, Gabet C, Belmonte T, Michel H et al (2001) Surf Coat Technol 142–144:241
18. Xu X, Yu Z, Wang L, Qiang J, Hei Z et al (2003) Surf Coat Technol 162:242
19. Grigull S, Parascandola S et al (2000) J Appl Phys 88:6925
20. Möller W, Parascandola S, Kruse O, Günzel R, Richter E et al (1999) Surf Coat Technol 116–119:1
21. Clausen B, Lorentzen T, Bourke M, Daymond M et al (1999) Mater Sci Eng A 259:17
22. Stinville J, Tromas C, Villechaise P, Templier C et al (2011) Scr Mater 64:37
23. Oddershede J, Christiansen T, Ståhl K, Somers M et al (2008) J Mater Sci 43:5358. doi:10.1007/s10853-008-2791-y
24. Oddershede J, Christiansen T, Ståhl K, Somers M et al (2010) Scr Mater 62:290
25. Taylor G (1938) J Inst Met 62:307
26. Winther G (2008) Mater Sci Eng A 483–484:40
27. Christiansen T, Somers M et al (2009) Metall Mater Trans A 40:1791
28. Czerwiec T, He H, Marcos G, Thiriet T, Weber S, Michel H et al (2009) Plasma Processes Polymers 6:401